Morphological design of alumina hollow fiber membranes for desalination by air gap membrane distillation

L. García-Fernández [1], Bo Wang [2,3], M.C. García-Payo [1], K. Li [2,3], M. Khayet [1,4,*]

[1] Department of Applied Physics I, Faculty of Physics, University Complutense of Madrid, Av. Complutense s/n, 28040, Madrid, Spain.

[2] Department of Chemical Engineering, Imperial College London, London SW7 2AZ, UK.

[3] Barrer Centre, Imperial College London, London SW7 2AZ, UK.

[4] Madrid Institute for Advanced Studies of Water (IMDEA Water Institute), Avda. Punto Com nº 2, Alcalá de Henares, 28805, Madrid (Spain).

* Corresponding author: khayetm@fis.ucm.es

Tel. +34-91-3945185

Fax. +34-91-3945191

Abstract

Alumina hollow fiber membranes were prepared by the phase inversion technique under different spinning conditions in order to induce various types of structural morphologies. In the membrane fabrication process, the studied parameters were the polymer concentration in the inorganic suspension and its flow rate, the gap distance, the bore liquid, the outer coagulant composition and their flow rates. After sintering, the hollow fibers were chemically modified by grafting (1H,1H,2H,2H-perfluorodecyltriethoxysilane) rendering them hydrophobic for their use in membrane distillation (MD) process. The effects of the membrane morphology on the obtained MD membrane characteristics and on air gap membrane distillation (AGMD) desalination performance were studied in order to figure out the most promising structure for MD. The suitability of alumina hollow fibers for AGMD was confirmed by various membrane characterization techniques. In general, the membranes prepared with lower polymer concentration in the inorganic suspension exhibited higher AGMD performance (i.e. higher permeate flux with a smaller flux reduction factor and a good salt rejection factor). Among all prepared hollow fiber membranes prepared in this study, the one with the largest micro-channel structure exhibited the best AGMD performance, even better than all hydrophobic ceramic membranes used so far in desalination by AGMD and DCMD.

Keywords: Alumina hollow fiber membrane; membrane morphology; grafting modification; Rayleigh-Taylor instability; membrane distillation; desalination.

1. Introduction

Water desalination by membrane distillation (MD) is an environmentally-friendly alternative able to tackle the global water scarcity issue in combination with other water treatment techniques [1-3]. MD process can be used to produce not only distilled water but also ultrapure water, and stands out for its capability to treat concentrated salt aqueous solutions [3-5]. Porous hydrophobic membranes are used in this non-isothermal process in which the driving force for the mass transfer is the transmembrane vapor pressure.

The majority of MD studies were performed with membranes made from hydrophobic polymers such as polyvinylidenefluoride (PVDF), polypropylene (PP) and polytetrafluoroethylene (PTFE) [5]. Ceramic membranes can endure harsh environments, opening up the possibility of treating a broader variety of feed solutions and operating conditions [6-10]. It is well known that the superior structural, thermal and chemical characteristics of these membranes, facilitate membrane cleaning process after fouling without reducing the membrane properties and maintain its lifetime as consequence reducing therefore the membrane´s replacement cost [11]. In spite of the excellent thermochemical stability of ceramic membranes, these are seldom explored for MD applications, mainly due to their hydrophilic nature. In other words, ceramic membranes cannot be used directly in MD, but are rendered hydrophobic by surface modification using diverse agents and techniques as described elsewhere [12]. This is one of the main limitations of using ceramic membranes in MD applications.

Different inorganic membranes of metal oxides (i.e. alumina, zirconia and titania) and non-oxides (i.e. silicon nitride) were used in desalination by MD. Research studies with commercial ceramic membranes have been carried out analyzing different properties such as the pore diameter of the zirconia layer on the microporous alumina tubular support [13], the grafting efficiency in terms of hydrophobic stability of the tubular titania

membrane with time [14] and the effect of modifying agent type on alumina anodisc^{TM} membranes [15]. Other research studies have been devoted to the preparation of ceramic membranes with different inorganic suspension compositions in order to perform the most promising one in MD [8, 16, 17]. Das et al. [16] studied the effect of the clay/alumina suspension proportions on the characteristics of the capillary membranes. By means of rheological properties, Zhang et al. [8] and Wang et al. [17] analyzed first the stability of silicon nitride and β-Sialon suspensions, respectively. Then, other parameters such as the powder/polymer binder ratio of the silicon nitride hollow fiber membranes and the β-Sialon hollow fiber composition and sintering temperature were investigated looking for the suitable properties of an MD membrane.

Other researches using ceramic membranes focused on the study of the effects of the MD operation parameters (i.e. sodium chloride concentration of the feed aqueous solution, feed and permeate temperatures and flow rates) [13, 18] and the different MD configurations (i.e. air gap membrane distillation (AGMD), direct contact membrane distillation (DCMD) and vacuum membrane distillation (VMD)) [8, 17, 19] on the desalination efficiency. In all cases, compared to the other MD configuration the VMD permeate flux was the highest. Zhang et al. [8] found a significant difference between VMD and DCMD permeate fluxes of the grafted silicon nitride hollow fiber membranes mainly due to the temperature polarization effect. Wang et al. [17] managed to reduce this difference by using β-Sialon ceramic membranes with a lower thermal conductivity, but VMD flux remained the highest. In VMD configuration, the mass transfer resistance is reduced due to the air removal from the membrane pores and the conductive heat loss through the membrane is the smallest compared to the other MD configurations. However, this configuration is not very attractive from an industrial point of view since external condensers are necessary to collect the distillate outside the membrane module,

complicating in this way the system assembly and increasing the operational cost [4]. Cerneaux et al. [19] also compared the VMD and DCMD permeate fluxes of the zirconia tubular membranes with those of AGMD configuration. In AGMD configuration, as a consequence of the high thermal conductivity of ceramic materials, the temperature at the permeate side of the membrane is higher than that registered when using polymeric membranes with lower thermal conductivity. However, owing to the low thermal conductivity of the air gap, the temperature of the condensing surface is kept low, leading to a higher effective temperature gradient than that observed in DCMD when using ceramic membranes and comparatively better water production rates are obtained in AGMD. In addition to the lower heat transfer by conduction through the membrane in AGMD than in DCMD [4], other advantage of AGMD is the less risk of membrane pore wetting [13]. Nevertheless, the ceramic membranes used so far in MD showed very low AGMD permeate fluxes [13, 14, 16, 18, 19].

It is worth quoting that very few MD studies have been performed in desalination by ceramic hollow fiber membranes. However, it is important to emphasize the competitive interest of this membrane configuration against tubular, capillary or flat-sheet due to its higher packing density in modules (i.e. up to 9000 m^2/m^3) [20, 21]. Among the proposed ceramic membrane materials, alumina is the most commonly used one because of its chemical and mechanical stability as well as its wide availability and low cost.

The majority of ceramic membranes used so far in desalination by MD are not hollow fibers and their MD performance is usually lower than that of polymeric membranes [12, 22]. Therefore, attempts have been made in this study to prepare ceramic hollow fiber membranes with different morphologies. The morphological characteristics of the membranes play a key role in MD performance [23-25]. However, the effect of the membrane morphology on MD performance has not been thoroughly studied yet for

ceramic membranes. As such, this work is focused on the preparation of alumina hollow fiber membranes with different morphological designs in order to figure out the suitable structure inducing better AGMD performance. The study of the effects of the alumina hollow fiber membrane morphology on the MD membrane characteristics and on the AGMD performance may give important new insights into the structure performance correlation in the MD field. It will be shown through proper structural morphologies that ceramic hollow fiber membranes have the potential to obtain high permeation flux competitive in desalination when using AGMD process.

2. Experimental

2.1 Materials

Aluminium oxide powders (Al_2O_3 Powder, Ultra-Pure Grade, 99.99%) with an average particle size of 0.5 – 1.0 μm were purchased from Inframat® Advanced Materials™. The polymeric binder was polyethersulfone (PESf, Radel A-300, Solvay Advanced Polymers GmbH, Dusseldorf, Germany). The additive was Arlacel P135 (polyethylene glycol 30-dipolyhydroxystearate, Uniqema, Wilton, UK). The solvent N-Methyl-2-pyrrolidone (NMP, GPR RECTAPUR, VWR Chemicals), ethanol (VWR Chemicals) and deionized (DI) water were used as coagulants. The grafting solution consists of 1H,1H,2H,2H-Perfluorodecyltriethoxysilane (97%, Sigma-Aldrich) and methanol (HiPerSolv CHROMANORM, VWR Chemicals). POREFIL® (Porometer) and isopropyl alcohol (IPA, Sigma-Aldrich Chemical) were the wetting liquids used for the gas-liquid displacement test and the void volume fraction measurement, respectively. The feed salt aqueous solutions of AGMD experiments were composed by sodium chloride (NaCl), which was purchased from Scharlab.

2.2 Preparation of alumina hollow fiber membranes

First, the spinning suspensions were prepared by dissolving 0.42 wt% of the dispersant (Arlacel P135) in 35.75 wt% of solvent (NMP) and then, the 63.83 wt% of aluminium oxide powder was added to the mixture. In order to obtain a good inorganic dispersion, the mixture was ball milled (SFM-1 Desk Top Planetary Ball Miller, MTI Corportation) with 40 zirconia milling balls of 8-mm for 7 days. Subsequently PESf was added in two different concentrations, 6 wt% (PESf/alumina ratio = 1/10, low polymer concentration, LP) and 10.6 wt% (PESf/alumina ratio = 1.9/10, high polymer concentration, HP). After the addition of PES, LP suspension was milled for a further 24 h and HP for 48 h. Once the homogeneous alumina suspensions were prepared, these were degassed under vacuum (Self-Cleaning Dry Vacuum System™, Model 2025, Welch®) with stirring (yellow^{line}, OST 20 digital, Veriserv) for approximately 3 h, and then transferred to a stainless steel syringe (200 mL). The bore liquid and the outer coagulant solutions were also introduced in stainless steel syringes of 200 mL and 100 mL, respectively. The flow rate of the fluids was controlled by infusion pumps (Harvard Apparatus, PHD 2000 Programmable and Chemyx Inc., Model Nexus 6000). The inorganic suspension, the bore liquid and the outer coagulant were simultaneously extruded vertically through a triple-orifice spinneret with diameters of 0.9, 2.6 and 3.5 mm, and fall into a DI water coagulation bath. The spinning parameters are summarized in Table 1. After spinning, the alumina hollow fiber membrane precursors were stored overnight in a DI water bath at room temperature to remove the residual solvent. Then, they were straightened and dried overnight at room temperature before calcination and sintering in air atmosphere (Carbolite RHF 1600 furnace) as follows. The temperature was raised from room temperature to 600 ^{o}C at 1 ^{o}C/min and kept for 3 h, and then it was increased from 600 ^{o}C to the target temperature (1450 ^{o}C) at 1 ^{o}C/min and hold for 5 h. Finally, it was reduced to room temperature at a

rate of 2 ºC/min. More details of inorganic suspension preparation and ceramic hollow fiber membrane fabrication can be found in previous studies [9, 26].

2.3 Modification of alumina hollow fiber membranes

The prepared ceramic hollow fiber membranes were hydrophilic in nature. For MD applications, these must be modified to become hydrophobic [6, 13]. The used grafting solution was composed by 2 vol.% of 1H,1H,2H,2H-perfluorodecyltriethoxysilane in methanol [18, 27]. Two stages conformed the experimental procedure: i)- the hollow fibers were soaked in the grafting solution under vacuum (Self-Cleaning Dry Vacuum System™, Model 2025, Welch®) for 30 min, and then dried in air (1 h) and in oven (1 h) (Thermocenter, SalvisLAB, John Godrich); ii)- the hollow fibers were soaked again under vacuum for 15 min and dried in air (1 h) and in oven (1 h). Due to the low surface tension of methanol and the applied vacuum during membrane soaking, the prepared alumina hollow fibers were rendered totally hydrophobic provided that the membrane pores were also filled with the grafting solution.

2.4 Characterization of alumina hollow fiber membranes

Both the inner and outer diameters as well as the thickness of the fibers were determined by a digital microscope (VHX, Keyence VH-Z100R) and the corresponding software (VHX-900F).The cross-section morphology together with the internal and the external surfaces structures of the prepared alumina hollow fiber membranes were analyzed by scanning electron microscopy (SEM, Gemini LEO 1525). All the samples were previously coated with gold.

Gas-liquid displacement porometer (Porolux™ 1000, Porometer) was used to determine the bubble pore size, the mean pore size and the smallest pore size of all the prepared hollow fiber membranes. The experimental porometry method was described elsewhere [28-30], Porefil® (Porometer) was used as the wetting liquid and pure nitrogen was the gas employed in this test. The mercury intrusion porosimetry (MIP) technique (Micromeritics AutoPore IV) was employed to obtain the pore size distribution of the membranes and the pore tortuosity factor. The applied pressure was between 3.45 10^4 and 2.28 10^8 Pa with an equilibration time of 10 s for the low pressure range and 20 s for the high pressure range. An angle of 130° was considered as the mercury advancing contact angle.

The overall void volume fraction (i.e. porosity) (ε) of the membranes was measured by the gravimetric method as described elsewhere [31] and calculated as follows:

$$\varepsilon = \frac{(m_w - m_d)/\rho_{IPA}}{(m_w - m_d)/\rho_{IPA} + m_d/\rho_{Al}} 100 \quad (1)$$

where m_w and m_d are the weighted mass of the membrane wetted by isopropyl alcohol (IPA) and the mass of the dry sample, respectively. ρ_{IPA} is the density of the wetting liquid IPA (0.785 g/cm^3, Sigma-Aldrich Chemical) and ρ_{Al} is the density of the alumina powder (3.97 g/cm^3, Inframat® Advanced Materials™).

The prepared hollow fiber membranes were also analyzed by Fourier transform infrared spectroscopy (FTIR) with a Nicolet iS50 device equipped with a beam splitter KBr, the detector DTSG-KBr and the accessory of attenuated total reflectance (ATR, SpectraTech Performer) with diamond crystal. The FTIR-ATR spectra were obtained by carrying out 128 scans with 8 cm^{-1} resolution.

The dynamic contact angles (θ) of the outer surface of the hollow fiber membranes were indirectly measured at room temperature by Wilhelmy balance method technique

[32, 33]. The fiber was first hung on the microbalance of the tensiometer (Kruss K100), and then immersed in DI water at a rate of 3 mm/min. The side of the fiber, which was immersed into the testing liquid, was closed with epoxy resin.

Liquid entry pressure of water (LEP_w) on the membranes was determined using the experimental set-up and the procedure described elsewhere [34]. This parameter together with the FTIR-ATR analysis and the dynamic contact angle are useful to confirm the hydrophobic character of the modified ceramic hollow fibers and to ensure their applicability in AGMD.

In general, the mechanical strength of the ceramic hollow fiber membranes is not altered with the grafting modification as it was previously confirmed elsewhere [33, 35]. Therefore, the mechanical strength was measured only for the original alumina hollow fibers by means of the three-point bending test, which was carried out using an Instron system (model 5543, Bluehill 3). Three samples of 30 mm long of each membrane were performed using a 1 kN load cell and a cross-head speed of 0.01 mm/s. The bending strength (σ_F) was calculated from the equation described elsewhere [36, 37] and the flexure test scheme and procedure was also shown in [38].

2.5 Air gap membrane distillation experiments

AGMD experiments were performed using the experimental device schematized in Fig. 1(a). The temperature of the feed solution (1) was controlled by a heating thermostat (2) (DT Heto) and a heat exchanger (4). The feed solution was circulated tangentially through the lumen side of the alumina hollow fiber membrane module (7) by means of a peristaltic pump (3) (Cole Parmer Masterflex easy-load model 7529-20). The shell side of the membrane module was cooled by a PolyScience chiller (8) in order to keep constant the temperature of the condensation surface. The tubular membrane module was set in a

tilted position (see Fig. 1(a)) and the permeate was collected from the bottom of the module. The mass of the produced water (9) and the inlet and outlet temperatures of the membrane module were determined by a balance (10) (AND GF-1200) and calibrated Pt-100 probes (6) connected to a multimeter (12) (Keithley 199 System DMM/SCANNER), respectively. Both the balance and the multimeter were connected to a computer (13), which registered the mass and temperatures measurements over time. All the experiments were carried out keeping both the inlet feed and cooling temperatures of the module at 80 ^{o}C and 20 ^{o}C, respectively. The feed flow rate was maintained at 35 L/h by means of a flow meter (11) (Tecfluid) and the hydrostatic pressure was controlled by a pressure gauge (5) (Wika), before the entrance of the liquid in the membrane module. The hollow fiber membrane module and all the elements of the set-up were thermally insulated. After ensuring that the membrane module had no leakage, the AGMD experiments were carried out using first distilled water as feed and then salt (NaCl) aqueous solutions of different concentrations (1.2, 3 and 6.5 wt%). The salt concentration of the feed and permeate solutions was measured during the experiments by an electrical conductivity meter (Metrohm model 712). The AGMD permeate flux (J) was obtained from the registered mass of the produced water (Δm) over time (Δt) and the internal surface area of the membrane (A_{in}). The permeate flux and the salt rejection factor (α) were calculated as follows:

$$J = \frac{\Delta m}{A_{in}\Delta t} \tag{2}$$

$$\alpha = \left(1 - \frac{C_p}{C_f}\right)100 \tag{3}$$

where C_p and C_f are the concentration of the permeate and feed solutions, respectively.

The permeate flux reduction factor (*FRF*) represents the relative difference between the obtained permeate flux when distilled water (J_w) and NaCl aqueous solution ($J_{NaCl\ wt\%}$) are used as feed. This parameter can be used to compare the efficiency of the membranes for the same NaCl feed solution and AGMD operating conditions. *FRF* for a given NaCl feed solution ($FRF_{NaCl\ wt\%}$) was determined by the following equation:

$$FRF_{NaCl\ wt\%}(\%) = \left(\frac{J_w - J_{NaCl\ wt\%}}{J_w}\right) \times 100 \quad (4)$$

The AGMD hollow fiber membrane module was specifically designed and fabricated for these experiments (see Fig. 1(b)). It is worth noting that this membrane module can be used for all MD configurations (i.e. DCMD, AGMD, sweeping gas membrane distillation (SGMD) and VMD). Three hydrophobic alumina hollow fibers were packed in a copper tube, which was coaxially placed inside the stainless-steel shell used as the cooling chamber. A three-holed cover (14) was welded at each end of the copper tube. Each hollow fiber was introduced through the corresponding holes of each top and bottom covers and then it was fixed with epoxy resin at both ends. The three-holed covers were designed to maintain parallel the hollow fibers inside the tubular module, keeping constant the space between them and the distance between the fibers and the copper condensation surface (16) (i.e. the radial minimum air gap distance (15) was 1 mm). The effective length of the AGMD tubular module was 120 mm.

3. Results and discussions

3.1 Structural characteristics

The inner and outer diameters as well as the thickness of the sintered ceramic hollow fiber membranes are summarized in Table 2. These parameters are significantly affected

by the viscosity of the ceramic suspension and the precipitation rate during spinning, which determine the resistance of the nascent fibers to gravity that induces elongation. In general, for the two used suspensions, the fibers made from the more viscous HP suspension, due to its higher polymer concentration, exhibited bigger diameters and thicker walls compared with the fibers made from the less viscous LP suspension when the same spinning parameters were considered. The minimum diameters (i.e. minimum MD membrane permeate surface) corresponded to the membrane LP2 and the maximum ones to the membrane HP3. This membrane exhibited the biggest external and internal diameters as it was prepared under a zero-gap distance using a weak non-solvent (40 wt% EtOH/60 wt% NMP) as a bore liquid. The highest and lowest thickness of these hollow fibers was determined for the membranes LP1 and LP4, respectively. The hollow fiber LP1 was prepared under a zero-gap distance and a strong non-solvent (i.e. water) in contact with both the inner and outer sides of fiber immediately after extrusion. The membrane LP4 was prepared under a wet-gap distance of 25 cm and the solvent NMP was circulated through the outer channel of the spinneret leading to a precipitation delay. It is well known that spinning with a longer gap distance increased the fiber elongation stress resulting in a thinner membrane [39]. This effect could be even intensified for a slowly coagulated hollow fiber membrane, which suffered more the stretching force during the long gap distance.

Other than the diameters and thickness, wall structure is crucial dictating the properties of the hollow fiber membrane. Tuning the structure of the hollow fiber membrane consists of manipulating the occurrence and arrangement of micro-channels in the wall, which largely determines the asymmetric structure and hence the transport resistance during MD process. The generation of micro-channels in ceramic hollow fibers is based on a spontaneous fingering process induced by the density difference between the inorganic

suspension and the coagulant. In other words, the Rayleigh-Taylor instability, which amplifies the interfacial disturbing waves, lead to the periodical irregular invasion of the light fluid into the heavy one [40-43]. Different types of accelerating front can cause the interpenetration of the two fluids [44], but in this case the main acceleration of the interface can be due to the fast exchange between solvent and non-solvent as demonstrated in [40]. When the phase inversion starts, a strong non-solvent (e.g. water) comes into contact with the inorganic suspension and consequently, the solvent outflow from the inorganic suspension to the non-solvent promotes the contraction of the inorganic suspension. This induces a highly accelerated movement of the interface between the inorganic suspension and the non-solvent towards the suspension side (i.e. Rayleigh-Taylor instability initiation). The interfacial accelerates towards the heavier fluid (i.e. inorganic suspension is heavier than the non-solvent) and the secondary condition of the Rayleigh-Taylor instability is then met. Therefore, the fingering process starts and the micro-channels are formed due to the invasion of the periodical micro-streams of the non-solvent in the ceramic suspension [40]. According to the Rayleigh-Taylor instability theory, the initial momentum and the number of micro-channels are mainly affected by the interfacial acceleration, which is in turn determined by the exchange rate of the solvent and non-solvent. In general, when the solvent/non-solvent exchange rate is fast, the initial momentum and the number of micro-channels would be higher, and vice versa. After initiation, the growth of the micro-channels is driven by the momentum of the invading micro-streams. The interaction between different factors such as the initial momentum, densities, viscosities, precipitation rate, etc. determine the final length and width of the micro-channels [40]. Commonly, the micro-channels grow perpendicular to the surface where its formation is initiated according to the physical nature of the Rayleigh-Taylor instability. During the micro-channel formation process,

when the momentum of the non-solvent micro-streams is dissipated, the micro-channels stop growing and a sponge-like layer will be formed. Dissipation of the momentum can be accomplished by two means, one is the consumption of the initial momentum by the friction in the deforming suspension surrounding the micro-streams, which is determined by the viscosity and precipitation of the suspension; the other happens when two sets of micro-streams meet from opposite directions, in this case, a sponge-like layer will be sandwiched in between the micro-channels in the precursors. The sponge-like layer is a tight layer after sintering and it contributes to the most of transport resistance. This sponge-like layer is also important to the mechanical property of the membranes, as a large amount of material is distributed in it. Immediately after the initiation of the micro-streams, the entrance of the micro-channels on the suspension/non-solvent interface starts to contract because of the tension surrounding the entrance. At the same time, the polymer content at the interface and the entrance start to precipitate due to solvent/non-solvent exchange. Hence, the final size of the entrance of the micro-channels is largely determined by the competition between the contraction and the precipitation speeds. In general, a faster precipitation rate of the interface and the micro-channel entrance would be favored to obtain bigger entrance sizes, and the entrance could be completely closed if the precipitation rate is slow. Based on above theories, the morphology and pore structure of the hollow fibers will be reasonably interpreted in the following sub-sections.

3.1.1 Morphology control of the prepared alumina hollow fiber membranes

Figures 2 and 3 show the SEM images of the cross-sections of the ceramic hollow fiber membranes. It can be observed that different morphologies were designed and prepared according to the spinning parameters summarized in Table 1. Figure 2 corresponds to the

morphologies of the alumina hollow fibers prepared with the LP suspension and Fig. 3 to those of the membranes prepared with HP suspension.

DI water was used as internal and external coagulants for LP1 membrane preparation. By using this strong coagulant, fast precipitation occurred simultaneously at the inner and outer layer of the hollow fiber and micro-channels grew from both sides of the membrane and met in the middle of the wall to form a sandwich structure.

The alumina hollow fiber membranes LP2 and LP3 were prepared employing a weak outer coagulant (i.e. 50 wt% ethanol/50 wt% NMP) along the short gap (i.e. 5 cm). Such combination of the spinning parameters led to slower overall precipitation of the nascent hollow fibers, and the elongation effect from gravity permitted the formation of a thinner membrane wall and smaller diameters of the hollow fibers compared with LP1. For the hollow fiber LP2, the weak outer coagulant increased the viscosity of the outer surface suspension of the nascent fiber along the short gap. When the fiber entered into the water bath, the increased viscosity induced a slower solvent/non-solvent exchange at the outer surface, which resulted in less micro-channels from the shell side. For the hollow fiber LP3, the velocity of the bore liquid water was increased considerably (i.e. the flow rate was increased to 15 ml/min compared to 10 ml/min for LP2). This increase of the flow rate enhanced the solvent/non-solvent exchange rate at the inner surface, therefore the micro-channels from the lumen side got higher initial momentum to grow faster and longer than that corresponding to the hollow fiber LP2, reaching finally the position next to the outer surface. As a consequence, the viscosity of the outer surface was increased further (owing to solvent/non-solvent exchange with the water in the micro-channels) before entering the water bath compared to LP2, and micro-channels from the shell side were not formed. The most different morphology was observed for the ceramic hollow fiber membrane LP4 (see Fig. 2). For this membrane a very high bore liquid (i.e. water)

flow rate of 30 ml/min was used during spinning. Higher bore liquid flow rate helped to remove the exchanged solvent accumulated near the interface at the bore liquid side, maintaining the higher initial concentration gradient of the solvent across the inorganic suspension/bore liquid (water) interface. Larger concentration gradients induced an enhancement of the solvent/non-solvent exchange rate. Due to this fastest precipitation rate at the lumen side, the micro-channels had the highest initial momentum to break through the outer surface. By using a pure solvent (i.e. NMP) as the outer liquid along a large gap distance (i.e. 25 cm), coagulation was avoided during this gap, giving enough time for the micro-channels to reach the external layer before falling into the water bath, resulting in open micro-channels at the outer side of the membrane. It is worthy to mention that the combination of a high bore liquid (i.e. water) flow rate and a long gap distance was commonly considered [45]. Although the micro-channels could reach the outmost layer, such breaking through the outer surface was not observed in these studies. It is speculated that the surface tension on the outer surface of the nascent fiber provides a force against the direction of micro-channel growth and therefore hindered the breaking process of the micro-channels. In our case, by flowing NMP on the outer surface, the tension of the outer surface of the nascent fiber was eliminated and consequently the micro-channels could break the surface easily.

The hollow fibers HP1 and HP2 used the same spinning parameters (except the inorganic suspension) as those of LP2 and LP3, respectively. The greater viscosity of the HP suspension reduced the solvent/non-solvent exchange rate and therefore the micro-channels had lower initial momentum to grow from the lumen side. Furthermore, the higher viscosity of the HP suspension dissipated the momentum faster than the LP suspension, inhibiting therefore the growth of micro-channels more efficiently [40]. As a consequence, despite the fact that HP1 and HP2 showed similar structures as LP2 and

LP3, respectively, the micro-channels at the lumen side are shorter and smaller than those of LP2 and LP3.

Completely different cross-section morphology was observed in Fig. 3 for the membrane HP3, when a weak non-solvent mixture was employed as a bore liquid (i.e. 40 wt% ethanol/60 wt% NMP) under a zero-gap distance. This coagulant induced a slow solvent/non-solvent exchange rate and precipitation at the lumen side, leading to a micro-channel free sponge-like structure at the inner layer of this fiber. On the one hand, micro-channel structure formation started at the shell side of the membrane HP3, owing to the fast solvent/non-solvent exchange induced by water in the coagulation bath. The micro-channels formed from the shell side stopped next to the inner surface due to momentum dissipation by the viscosity and the slow precipitation of the suspension at the lumen side.

3.1.2 Pore structure of the prepared alumina hollow fiber membranes

The bubble, mean and smallest pore sizes of the alumina hollow fiber membranes were determined by gas-liquid displacement test. These results are summarized in Table 3. All membranes exhibited similar pore sizes, except the hollow fiber LP4, which had significantly larger pore sizes due to its unique structure. The average mean pore size of the other alumina hollow fiber membranes were (233 ± 8) nm. This is an adequate pore size for MD membranes [4, 46]. Another suitable characteristic of an MD membrane is a narrow pore size distribution [4, 24]. The hollow fibers prepared in this study met this requirement (except the membrane LP4). The maximum difference between the bubble pore sizes and the smallest pore sizes (i.e. the widest pore size distribution) was 205 nm for the hollow fiber HP3, which was prepared with a high concentration of solvent in the bore liquid mixture (40 wt% ethanol/60 wt% NMP). Comparatively, Zhang et al. [47] prepared yttria-stabilized zirconia (YSZ) hollow fiber membranes with a wider pore size

distribution when higher NMP content was used in the bore liquid mixture (i.e. NMP/water). The bubble pore sizes and the smallest pore sizes of the original hollow fiber membranes LP2 and LP3 differed only by about 50 nm. This means that both membranes had the narrowest pore size distributions.

Gas-liquid displacement only detects the effective open pore size, which is the 2-D projection of the real pore structure. However, it does not provide the full information of the 3-D hierarchical pore structure. On the other hand, MIP gives full information of the pore structure, but it does not permit to get an effective open pore size. Therefore, it is important to combine these two techniques to obtain a clear view of the pore structure. Figure 4 shows the pore size distributions (PSD) of the prepared alumina hollow fiber membranes determined by MIP analysis. All the hollow fibers showed a hierarchical pore structure consisting of more than one pore size including the inter-granule pore size between alumina particles and the micro-channel entrance pore size at different pore structure levels. All fibers have a common pore size with a first peak around 247 nm, which corresponds to the primary inter-granule pores between alumina particles. This is the smallest pores at the lowest level in the ceramic matrix, and it is close to the mean pore size determined by the gas-liquid displacement technique, except that of the hollow fiber LP4. This means that the effective open pore size is determined by the primary inter-granule voids. As it can be seen in Fig. 4(a), LP1 showed an additional peak around 324 nm, which corresponds to the size of the entrance of the micro-channels. Similarly, LP2 presented an entrance size of the micro-channels at 480 nm, and LP3 at 735 nm. The change of the size of the micro-channel entrance is related to the precipitation rate of the surfaces, as it will be explained later on. For the hollow fibers LP1 and LP2, the flow rate of the bore liquid water was the same, 10 ml/min, but the inorganic suspension flow rate and the gap distance were different. The hollow fiber membrane LP1 was prepared using

a higher inorganic suspension flow rate (15 ml/min compared to 8 ml/min employed for LP2) and zero gap distance, inducing a greater thickness after extrusion and reducing the solvent/non-solvent exchange rate as consequence. When using a higher extrusion rate, the non-solvent/solvent ratio exchanged during the spinning was lower, leading to a slower precipitation rate. Therefore, the micro-channel entrance had more time to contract before solidification resulting in a smaller size than that of LP2. The hollow fiber LP3 used a higher flow rate of the water bore liquid than LP2 leading to a higher precipitation rate of the inner surface and hence larger micro-channel entrance size than LP2. Compared with LP1, LP2 and LP3, the hollow fiber LP4 did not show any predominant secondary peak, but had a broaden pore size distribution ranging from tens of microns to sub-micron. This unique distribution corresponded to the open micro-channel structure of LP4. As the open micro-channels of LP4 have a conical shape, during MIP measurement, mercury was pushed into the big openings at low pressures, and the penetrated mercury volume increased smoothly when the pressure was increased. Then the incremental intrusion volume was kept small for each pressure increment, leading to a broaden pore size distribution. The size of the micro-channel entrances at the inner surface of LP4 could not be detected by the MIP technique, because it was the last part penetrated by mercury and the volume increase corresponding to this part is too small to produce a meaningful signal. The micro-channel entrance pore sizes can only be measured by the gas-liquid displacement technique, which determined a mean pore size of 537 nm. Although a higher bore liquid water flow rate was used for the LP4 fiber spinning its micro-channel entrance pore size was smaller than that of the hollow fiber LP3. The precipitation rate at the inner surface of the hollow fiber LP4 might be slowed down by the solvent used as outer coagulant. Figure 4(b) shows the PSD of the alumina hollow fiber membranes prepared with HP suspension. In addition to the primary inter-

granule pore size, the HP fibers exhibited another peak around 306 nm. This indicated that part of inter-granule pores between alumina particles were expanded due to the higher polymer concentration used for the HP suspension preparation. Furthermore, these fibers presented an additional peak around 362 nm, corresponding to the entrance size of the micro-channels. The incremental intrusion volume of this peak is greater for the membrane HP2 than for the other fibers, owing to the numerous and bigger micro-channels through its cross-section. This micro-channel entrance size was smaller than that of the membrane LP3 (prepared under the same spinning conditions) because of the higher viscosity (i.e. slower solvent/non-solvent exchange rate) of the HP suspension. It is worth noting that the inter-granule pore sizes of the prepared hollow fiber membranes were of the same order of magnitude as that reported by Lee et al. [48] for the alumina hollow fiber prepared with the same powder size, 1 μm, and sintered at the same temperature, 1450 ^{o}C.

The tortuosity of the membrane pores was also determined by MIP analysis. As it can be seen in Table 4, no significant changes were observed for the tortuosity factors of all prepared ceramic hollow fiber membranes. All obtained values were lower than 2, which is the value commonly considered for the tortuosity factor of MD membranes to carry out the permeate flux predictions [4]. The lowest value corresponded to the hollow fiber LP3 while the greatest one was obtained for HP3.

The void volume fraction of the prepared alumina hollow fiber membranes was determined by means of the gravimetric method, and the results are shown in Table 4. The highest porosity was obtained for the hollow fiber membrane LP4, which exhibited the largest pore sizes (see Table 3) and open micro-channels at the outer side (see Fig. 2). The other membranes had similar void volume fraction values around 52%. The hollow

fibers LP2 and LP3 showed slightly higher void volume fraction values. This is attributed partly to their larger micro-channel structures through their cross-sections (see Fig. 2).

3.1.3 Surface morphology and hydrophobicity of the membranes after grafting

Figures 5 and 6 show the SEM images of the inner and outer surfaces of the alumina hollow fiber membranes prepared with LP and HP suspensions, respectively. In general, the surface is more porous if the nascent surface is brought in contact with the non-solvent immediately after extrusion, while the surface becomes denser if the nascent surface experiences an air gap distance. The former case applied to all inner surfaces and the outer surface of LP1 and HP3, while the later case applied to the outer surface of LP2, LP3, HP1 and HP2. Similar results were described elsewhere [49, 50]. An exception was the outer surface morphology of the membrane LP4 (see Fig. 5), which presented very large pores due to the open micro-channels at the outer side of the fiber.

By comparing the hollow fiber membranes prepared under the same spinning conditions but with different polymer concentrations in the inorganic suspension (compare the fibers HP1 and HP2 in Figs. 5 with LP2 and LP3 in Fig. 6, respectively), quite similar porous surface morphologies can be observed for these pairs of membranes. Although it is reasonable to link the surface porosity to the number and size of the micro-channel entrances on the surface, subtle changes in the pore size are difficult to distinguish by means of SEM, while the MIP results in Fig. 4 are more sensitive to the changes. It should be noted that the membrane HP3 has a rougher inner surface than other samples (see Fig. 6) despite the fact that there is no micro-channels generated from the inner surface. This should be attributed to the high content of solvent in the bore liquid that led to erosion of the nascent fiber inner surface and the loss of some ceramic material. Such

eroded morphologies were also observed in other ceramic hollow fibers when high-solvent bore liquids were used during fabrication [51].

Both the internal and external surfaces of the grafted alumina hollow fiber membranes were also analyzed by SEM. As it was expected, no significant changes were observed when comparing the surfaces of the grafted alumina membranes to those of the corresponding original ones. In fact, the followed grafting modification technique changed only the chemistry of the ceramic membrane as it was observed in previous studies [6, 33]. Hendren et al. [15] employed different chemicals to modify the hydrophobicity of alumina anodisc^{TM} membranes for their application in MD. For the same chemical used in the present study (i.e. 1H,1H,2H,2H-perfluorodecyltriethoxysilane), the pores of the membrane surface were not blocked as shown by the SEM images. Consequently, other properties such as the pore size and porosity of the prepared hollow fiber membranes were not altered after grafting modification (see Tables 3 and 4).

The grafting efficiency of the alumina hollow fiber membranes by the perfluoroalkylsilane modification agent was studied by FTIR-ATR, water contact angle and LEP_w characterization techniques [6, 7, 14, 16, 19, 33, 52-55]. Figure 7 shows the FTIR-ATR spectra (a) and (b) together with the water contact angle measurements (c) of the original and grafted membranes. For both types of membranes (i.e. LP and HP fibers), successful grafting modification was carried out because the absorption bands of the alkylsilanes were detected at the wavenumbers range, 1300 – 975 cm^{-1}. The specific vibration bands of the perfluorinated chains were also observed by several authors [6, 14, 16, 19, 55]. Different infrared absorption bands can be distinguished: fluoro-carbon chains ($–CF_2$, $–CF_3$) at 1242 cm^{-1}; $–Si-O–C_2H_4–C_xF_{2x+1}$ group at 1206 and 1150 cm^{-1} and the vibration of –Si–O– bond at 1112 cm^{-1}. Similar vibration bands were found by Kujawa

et al. [55] for the grafted alumina powders using the same modification agent used in this study (i.e. 1H,1H,2H,2H-perfluorodecyltriethoxysilane, C8).

The hydrophobicity of both the original and modified hollow fiber membranes was analyzed by means of the water contact angle measurements (Figure 7(c)). The considered grafting modification technique proved to be very effective because it changed the intrinsic hydrophilic nature of the alumina membranes (i.e. $(57 \pm 8)^{o}$ is the average water contact angle of the original fibers) to be hydrophobic (i.e. $\theta > 90^{o}$, $(147 \pm 9)^{o}$ is the average water contact angle of the grafted fibers). Some hollow fibers were rendered superhydrophobic (i.e. $\theta > 150^{o}$ of the hollow fibers LP2, LP3 and HP3). The water contact angles of the grafted membranes in this study were higher than those determined for other grafted alumina hollow fibers (i.e. contact angles lower than 120^{o}) [33]. It is well known that the grafting method consists on a chemically bonding between the hydrolysable groups of the modified agent and the hydroxyl groups of the ceramic membranes. The number of the functional groups of the modified agent structure is one of the parameters that directly affects the grafting efficiency. Hendren et al. [15] demonstrated that the grafting success of the 1H,1H,2H,2H-perfluorodecyltriethoxysilane was due to the three available functional sites of each molecule. It is worth noting that the lowest contact angle measurement and the highest experimental uncertainty were registered for the membrane LP4. This was in agreement with the extremely large pores observed on its outer surface (see Fig. 5).

The hydrophobic character and consequently the MD applicability of the grafted hollow fiber membranes were confirmed by measuring LEP_w. This technique was also used by several authors to control the efficiency of the grafting modification of the ceramic membranes (hollow, capillary and tubular) with different perfluoroalkylsilane molecules and grafting procedures [6, 7, 14, 16, 19, 53, 54]. All the measured LEP_w values

of the prepared membranes were higher than 3.8 10^5 Pa, which is the maximum pressure limit of the experimental device, except that of the hollow fiber LP4. The LEP_w value of this membrane was 0.3 10^5 Pa. This lowest LEP_w value could be due to some defects found in the membrane structure corresponding to open micro-channels passing through the entire fiber cross-section. Therefore, all hollow fibers, except LP4, can be used in AGMD without any wetting problem as the applied transmembrane hydrostatic pressure was lower than the LEP_w values. It is worth quoting that the obtained LEP_w values were higher than those reported for other modified alumina hollow fiber membranes used in desalination by MD, which were around 1-1.5 10^5 Pa [6, 16]. However, the LEP_w values obtained for some grafted zirconia and titania membranes reached up to 9 10^5 Pa and 10^6 Pa [14, 19].

3.2 Mechanical property of the prepared alumina hollow fibers

It is important to guarantee a good mechanical strength of the hollow fiber membranes in order to ensure their good packing in tubular modules for MD applications. The bending strengths of the original alumina hollow fibers are summarized in Table 5. The bending strength of all prepared alumina membranes were within the range (50 – 250 MPa) reported previously by Koonaphapdeelert and Li [33] for alumina hollow fibers sintered under the target temperatures 1400 and 1500 ^oC. The hollow fiber HP3 exhibited the highest bending strength attributed partly to the lower number of micro-channels in its structure. Lee et al. [37] stated that the mechanical properties of the hollow fiber membranes were reduced with the formation of micro-channel structures. This is corroborated by the membrane LP4 having the lowest bending strength and large micro-channels through the fiber cross-section, which were opened at its outer surface (see Fig. 2 and 5).

3.3 AGMD experiments of the grafted alumina hollow fiber membranes

The AGMD performance of all the grafted alumina hollow fiber membranes is shown in Fig. 8. The permeate fluxes (J, Fig. 8(a)) as well as both the salt rejection and flux reduction factors (α and $FRF_{NaCl\ 3wt\%}$, Fig. 8(b)) were related with the morphology and characteristics of the prepared hollow fiber membranes. The structural design of the hollow fiber LP4 provided the highest permeate flux in this study, which was significantly greater than those obtained from the other membranes (see Fig. 8(a)). This membrane exhibited the highest porosity, the largest pore size, and the lowest thickness as a consequence of the open micro-channel structures at the outer side of this fiber (i.e. big pores of the outer surface). However, not only was the water vapor transported through the membrane pores, but the feed solution also crossed the entire membrane wall through some defects (i.e. micro-channels opened at both inner and outer layers). Apart from increasing the permeate flux, these defects reduced both the resultant salt rejection factor (i.e. 97.97%) and the $FRF_{NaCl\ 3wt\%}$ of the hollow fiber LP4 to the minimum values of this study as shown in Fig. 8(b). This result was anticipated since the hydrostatic pressure of these AGMD experiments was 0.3 10^5 Pa, coinciding with the LEP_w of this hollow fiber. Therefore, it can be concluded that the hollow fiber membrane LP4 is not an adequate membrane for MD applications. Nevertheless, in spite of its low salt rejection factor, the average concentration of the permeate solution was 0.54 g/L, which is slightly higher than the concentration limit of drinking water (i.e. 0.5 g/L) [56].

In general, among the other hollow fiber membranes, the LP fibers exhibited greater permeate fluxes than those of the HP fibers. Particularly, it can be clearly seen that the permeate fluxes of the hollow fiber membranes prepared under the same spinning conditions but with the lower polymer concentration in the inorganic suspension were

higher (compare the membranes LP2 with HP1 and LP3 with HP2 in Fig. 8(a)). This is related with the morphological difference between the LP and HP hollow fibers, where LP fibers have longer, bigger and more micro-channels than the HP hollow fibers, which have thicker and tighter sponge-like structure with less micro-channels. The large micro-channels provided better AGMD permeate flux because this kind of structure reduced more the heat transfer by conduction following Fourier´s law and consequently the mass transport resistance through the membrane than that of the tight sponge-like structure. The lowest AGMD performance was observed for the hollow fiber HP3, whereas the highest one was registered for the hollow fibers LP2 and LP3.

The hollow fiber HP3 had the minimum permeate flux mainly because this membrane had less number of micro-channels and a sponge-like structure at the inner layer, resulting in a membrane with a higher thermal conductivity coefficient. Furthermore, this membrane had the highest tortuosity factor (see Table 4), which contributed also to the reduction of the permeate flux.

The hollow fibers LP2 and LP3 exhibited similar characteristics, which resulted in an improved AGMD permeate fluxes compared with the other hollow fiber membranes. These hollow fibers had bigger micro-channels, thinner wall, larger entrance size of micro-channels at the lumen side and slightly greater void volume fractions. As it is well known, the large micro-channels and the high porosities reduce both the vapor transport resistance across the fiber and the thermal conductivity of these membranes. Moreover, the hollow fiber membrane LP3 had larger micro-channels and lower tortuosity factor, leading to a slightly greater permeate flux than that obtained for the hollow fiber LP2. When comparing the AGMD permeate fluxes of the prepared grafted hollow fiber membranes (Fig. 8(a)) with those reported for other hydrophobic ceramic membranes used in different MD configurations (see Table 6), it can be demonstrated the excellent

water production rates of the hollow fiber membranes prepared in the present study. The resultant permeate fluxes obtained in this study were generally greater than the majority of those summarized in Table 6 and significantly higher than those used in AGMD configuration. Only the VMD permeate fluxes obtained for the grafted alumina hollow fiber membrane prepared by Fang et al. [6] were higher than the best AGMD permeate flux prepared in this study (i.e. LP3 in Fig. 8(a)). In fact, VMD configuration usually leads to higher permeate fluxes than those obtained in other MD configurations such as DCMD and AGMD (see Table 6 for some comparative studies [8, 17, 19]). Furthermore, VMD configuration requires a more complicated system design and a higher energy consumption [4].

As it can be seen in Fig. 8(a), by using distilled water as feed the permeate fluxes of all the hollow fiber membranes were slightly higher than those obtained with feed salt aqueous solution, resulting in low $FRF_{Nacl\ 3wt\%}$ as presented in Fig. 8(b). All the $FRF_{NaCl\ 3wt\%}$ values of the prepared hollow fibers were lower than 6%, except the membrane HP3, which had the highest $FRF_{NaCl\ 3wt\%}$ attributed partly to its lower water permeate flux compared to the other alumina hollow fibers.

In addition to the good AGMD permeate fluxes and $FRF_{NaCl\ 3wt\%}$, excellent salt rejection factors were obtained (i.e. higher than 99.988%). This means that the salt concentrations of the permeate solutions were lower than $3\ 10^{-3}$ g/L indicating the high purity of the produced water by AGMD with the prepared grafted alumina hollow fiber membranes. The hollow fiber membranes LP1 and LP3 had the greatest salt rejection factor (i.e. 99.995%). Their AGMD performance was further analyzed using feed aqueous solutions of different NaCl concentrations (i.e. 0, 1.2, 3 and 6.5 wt%). The resultant permeate fluxes are plotted in Fig. 9. As it was expected, the AGMD permeate flux decreased with the increase of the feed NaCl concentration. However, the obtained

permeate flux reduction was very low for both LP1 and LP3 membranes, because even for the highest feed salt concentration (i.e. 6.5 wt%, NaCl), the corresponding $FRF_{NaCl\ 6.5wt\%}$ were only 5.6 and 7.2%, respectively. Furthermore, the salt rejection factors were higher than 99.985% for all the AGMD experiments being the permeate concentrations lower than 2.3 10^{-3} g/L. These experiments demonstrated the promising applicability of the grafted alumina hollow fiber membranes for the treatment of brines. The obtained $FRF_{NaCl\ 6.5\ wt\%}$ results were significantly better (i.e. lower) than the following $FRF_{NaCl\ 6wt\%}$ values calculated for other grafted ceramic membranes tested in desalination by MD: 13.3% in [13] for AGMD; 20.6% in [57] for DCMD; 32.8% and 35.4% in [8] for DCMD and VMD, respectively (see details in Table 6).

Appropriate membranes for desalination by MD must exhibit a high permeate flux and salt rejection as well as a low flux reduction factor. Therefore, the hollow fiber LP3 formed by large micro-channel structures, provided the best AGMD performance in this study and it is well ranked between the MD ceramic membranes used in desalination (see Table 6).

4. Conclusions

Alumina hollow fiber membranes with different morphologies were prepared and modified for desalination by AGMD. The spinning parameters were manipulated in order to obtain the desired membrane structures, based on the well-recognized Rayleigh-Taylor instability theory. The effects of these morphological structures on the characteristics and performance of the membranes were thoroughly analyzed for the first time.

The prepared hollow fiber membranes exhibited two types of pores: the primary inter-granule pores between alumina particles, which coincided with the effective open pores through the membrane; and the micro-channel entrance pores, related to each membrane

morphology. The majority of the alumina hollow fiber membranes obtained similar mean pore sizes and porosities (about 233 nm and 52%, respectively), which were within the range of MD applicability. The tortuosity values of the membrane pores were lower than two, which is a good factor for MD membranes. Furthermore, all the prepared alumina membranes provided suitable mechanical properties for packing in tubular modules.

The alumina hollow fiber membranes were successfully modified by grafting, rendering them hydrophobic (i.e. water contact angles higher than 136°) without altering any other membrane characteristics. The membranes LP2, LP3 and HP3 were superhydrophobic (i.e. water contact angles higher than 150°). Except the hollow fiber LP4, none of the grafted membranes showed any wetting problems (i.e. LEP_w values greater than 3.8 10^5 Pa). Therefore, excellent salt rejection factors (i.e. higher than 99.985%) and *FRF* values were obtained for desalination by AGMD. It is worth noting that the LP fibers prepared with the low polymer concentration in the inorganic suspension exhibited greater desalination performance (i.e. higher permeate flux and salt rejection factor as well as lower $FRF_{NaCl\ 3wt\%}$) than the HP fibers prepared with the high polymer concentration in the inorganic suspension. The best AGMD performance was obtained for the hollow fiber LP3 with large micro-channel structure and good characteristics (i.e. lower thickness, slightly higher void volume fraction and the lowest pore tortuosity factor) that reduced the mass transport resistance. Therefore, as a main conclusion of this study, it should be emphasized that the micro-channel structure is a suitable morphology to be adopted in ceramic hollow fiber membranes for AGMD.

In general, compared to the hydrophobic ceramic membranes used so far in desalination by MD, the grafted alumina hollow fiber membranes proposed in this study have excellent AGMD performance. Based on the MD results of these alumina hollow fibers, in particular to the excellent AGMD performance when highly concentrated salt

aqueous solution was used as feed, it can be drawn that brine water treatment by AGMD may be a potential application of these ceramic membranes. Furthermore, in accordance with the well-known excellent chemical resistance of the ceramic materials, long-term AGMD experiments could be carried out with the prepared grafted membranes in order to investigate their operating life and their fouling behavior.

Acknowledgements

The authors gratefully acknowledge the financial support of the Ministry of Economy and Competitiveness (MINECO) (CTM2015-65348-C2-2-R). L. García-Fernández is thankful to the Ministry of Education, Culture and Sports, Spain (MECD) for the FPU grant (FPU12/02817) and for supporting her research stay at Imperial College London.

References

[1] F. Macedonio, E. Drioli, A.A. Gusev, A. Bardow, R. Semiat, M. Kurihara, Efficient technologies for worldwide clean water supply, Chem. Eng. Process.: Process Intensification 51 (2012) 2-17.

[2] A. Chafidz, E.D. Kerme, I. Wazeer, Y. Khalid, A. Ajbar, S.M. Al-Zahrani, Design and fabrication of a portable and hybrid solar-powered membrane distillation system, J. Cleaner Prod. 133 (2016) 631-647.

[3] P. Wang, T.S. Chung, Recent advances in membrane distillation processes: Membrane development, configuration design and application exploring, J. Membr. Sci. 474 (2015) 39-56.

[4] M. Khayet, T. Matsuura, Membrane distillation: Principles and applications, Elsevier, The Netherlands, 2011.

[5] Y. Zhang, Y. Peng, S. Ji, Z. Li, P. Chen, Review of thermal efficiency and heat recycling in membrane distillation processes, Desalination 367 (2015) 223-239.

[6] H. Fang, J.F. Gao, H.T. Wang, C.S. Chen, Hydrophobic porous alumina hollow fiber for water desalination via membrane distillation process, J. Membr. Sci. 403-404 (2012) 41-46.

[7] W. Kujawski, J. Kujawa, E. Wierzbowska, S. Cerneaux, M. Bryjak, J. Kujawski, Influence of hydrophobization conditions and ceramic membranes pore size on their properties in vacuum membrane distillation of water–organic solvent mixtures, J. Membr. Sci. 499 (2016) 442-451.

[8] J.W. Zhang, H. Fang, J.W. Wang, L.Y. Hao, X. Xu, C.S. Chen, Preparation and characterization of silicon nitride hollow fiber membranes for seawater desalination, J. Membr. Sci. 450 (2014) 197-206.

[9] A.F. Ismail, K. Li, From Polymeric Precursors to Hollow Fiber Carbon and Ceramic Membranes, Membr. Sci. Technol. 13 (2008) 81-119.

[10] K.R. Reddy, M. Hassan, V.G. Gomes, Hybrid nanostructures based on titanium dioxide for enhanced photocatalysis, Appl. Catal., A: Gen. 489 (2015) 1-16.

[11] M. Lee, Z. Wu, R. Wang, K. Li, Micro-structured alumina hollow fibre membranes – Potential applications in wastewater treatment, J. Membr. Sci. 461 (2014) 39-48.

[12] E. Drioli, A. Ali, F. Macedonio, Membrane distillation: Recent developments and perspectives, Desalination 356 (2015) 56-84.

[13] S. Krajewski, W. Kujawski, M. Bukowska, C. Picard, A. Larbot, Application of fluoroalkylsilanes (FAS) grafted ceramic membranes in membrane distillation process of NaCl solutions, J. Membr. Sci. 281 (2006) 253-259.

[14] J. Kujawa, S. Cerneaux, W. Kujawski, Investigation of the stability of metal oxide powders and ceramic membranes grafted by perfluoroalkylsilanes, Colloids Surf., A 443 (2014) 109-117.

[15] Z.D. Hendren, J. Brant, M.R. Wiesner, Surface modification of nanostructured ceramic membranes for direct contact membrane distillation, J. Membr. Sci. 331 (2009) 1-10.

[16] R. Das, K. Sondhi, S. Majumdar, S. Sarkar, Development of hydrophobic clay–alumina based capillary membrane for desalination of brine by membrane distillation, J. Asian Ceram. Soc. 4 (2016) 243-251.

[17] J.W. Wang, L. Li, J.W. Zhang, X. Xu, C.S. Chen, β-Sialon ceramic hollow fiber membranes with high strength and low thermal conductivity for membrane distillation, J. Eur. Ceram. Soc. 36 (2016) 59-65.

[18] L. Gazagnes, S. Cerneaux, M. Persin, E. Prouzet, A. Larbot, Desalination of sodium chloride solutions and seawater with hydrophobic ceramic membranes, Desalination 217 (2007) 260-266.

[19] S. Cerneaux, I. Strużyńska, W.M. Kujawski, M. Persin, A. Larbot, Comparison of various membrane distillation methods for desalination using hydrophobic ceramic membranes, J. Membr. Sci. 337 (2009) 55-60.

[20] L. García-Fernández, M. Khayet, M.C. García-Payo, Membranes used in membrane distillation: preparation and characterization, in: A. Basile, A. Figoli, M. Khayet (Eds.) Pervaporation, Vapour Permeation and Membrane Distillation: Principles and Applications, Elsevier (Woodhead Publishing), Cambridge, 2015, pp. 317-359.

[21] X. Zhang, B. Lin, Y. Ling, Y. Dong, D. Fang, G. Meng, X. Liu, Highly permeable porous YSZ hollow fiber membrane prepared using ethanol as external coagulant, J. Alloys Compd. 494 (2010) 366-371.

[22] L.F. Dumée, S. Smart, M.C. Duke, S.R. Gray, Next generation membranes for membrane distillation and future prospects, in: A. Basile, A. Figoli, M. Khayet (Eds.) Pervaporation, Vapour Permeation and Membrane Distillation: Principles and Applications, Elsevier (Woodhead Publishing), Cambridge, 2015, pp. 415-447.

[23] M. Gryta, M. Barancewicz, Influence of morphology of PVDF capillary membranes on the performance of direct contact membrane distillation, J. Membr. Sci. 358 (2010) 158-167.

[24] M. Khayet, Membranes and theoretical modeling of membrane distillation: a review, Adv. Colloid Interface Sci. 164 (2011) 56-88.

[25] P. Wang, M.M. Teoh, T.S. Chung, Morphological architecture of dual-layer hollow fiber for membrane distillation with higher desalination performance, Water Res. 45 (2011) 5489-5500.

[26] B.F.K. Kingsbury, Z. Wu, K. Li, A morphological study of ceramic hollow fibre membranes: A perspective on multifunctional catalytic membrane reactors, Catal. Today 156 (2010) 306-315.

[27] H. Cao, H. Zheng, J. Yin, Y. Lu, S. Wu, X. Wu, B. Li, Mg(OH)2 Complex Nanostructures with Superhydrophobicity and Flame Retardant Effects, J. Phys. Chem. C 114 (2010) 17362-17368.

[28] X. Yang, R. Wang, L. Shi, A.G. Fane, M. Debowski, Performance improvement of PVDF hollow fiber-based membrane distillation process, J. Membr. Sci. 369 (2011) 437-447.

[29] L. García-Fernández, M.C. García-Payo, M. Khayet, Effects of mixed solvents on the structural morphology and membrane distillation performance of PVDF-HFP hollow fiber membranes, J. Membr. Sci. 468 (2014) 324-338.

[30] M. Essalhi, M. Khayet, Self-sustained webs of polyvinylidene fluoride electrospun nano-fibers: Effects of polymer concentration and desalination by direct contact membrane distillation, J. Membr. Sci. 454 (2014) 133-143.

[31] X. Li, C. Wang, Y. Yang, X. Wang, M. Zhu, B.S. Hsiao, Dual-biomimetic superhydrophobic electrospun polystyrene nanofibrous membranes for membrane distillation, ACS Appl. Mater. Interfaces 6 (2014) 2423-2430.

[32] Y. Yuan, T.R. Lee, Contact Angle and Wetting Properties, in: G. Bracco, B. Holst (Eds.) Surface Science Techniques, Springer-Verlag Berlin Heidelberg 2013, pp. 3-34.

[33] S. Koonaphapdeelert, K. Li, Preparation and characterization of hydrophobic ceramic hollow fibre membrane, J. Membr. Sci. 291 (2007) 70-76.

[34] M.C. García-Payo, M. Essalhi, M. Khayet, Effects of PVDF-HFP concentration on membrane distillation performance and structural morphology of hollow fiber membranes, J. Membr. Sci. 347 (2010) 209-219.

[35] C.C. Wei, K. Li, Preparation and Characterization of a Robust and Hydrophobic Ceramic Membrane via an Improved Surface Grafting Technique, Ind. Eng. Chem. Res. 48 (2009) 3446-3452.

[36] S. Liu, K. Li, R. Hughes, Preparation of porous aluminium oxide (Al2O3) hollow fibre membranes by a combined phase-inversion and sintering method, Ceram. Int. 29 (2003) 875-881.

[37] M. Lee, B. Wang, K. Li, New designs of ceramic hollow fibres toward broadened applications, J. Membr. Sci. 503 (2016) 48-58.

[38] K. Wang, A.A. Abdalla, M.A. Khaleel, N. Hilal, M.K. Khraisheh, Mechanical properties of water desalination and wastewater treatment membranes, Desalination 401 (2017) 190-205.

[39] M. Khayet, The effects of air gap length on the internal and external morphology of hollow fiber membranes, Chem. Eng. Sci. 58 (2003) 3091-3104.

[40] M. Lee, B. Wang, Z. Wu, K. Li, Formation of micro-channels in ceramic membranes – Spatial structure, simulation, and potential use in water treatment, J. Membr. Sci. 483 (2015) 1-14.

[41] D.J. Lewis, The Instability of Liquid Surfaces when Accelerated in a Direction Perpendicular to their Planes. II, Proc. R. Soc. Lond. Ser. A Math. Phys. Sci. 202 (1950) 81-96.

[42] D.H. Sharp, An overview of Rayleigh-Taylor instability, Physica D 12 (1984) 3-18.

[43] G. Taylor, The Instability of Liquid Surfaces when Accelerated in a Direction Perpendicular to their Planes. I, Proc. R. Soc. Lond. Ser. A Math. Phys. Sci. 201 (1950) 192-196.

[44] H.J. Kull, Theory of the Rayleigh-Taylor instability, Phys. Rep. 206 (1991) 197-325.

[45] B.F.K. Kingsbury, K. Li, A morphological study of ceramic hollow fibre membranes, J. Membr. Sci. 328 (2009) 134-140.

[46] M. Mulder, Basic Principle of Membrane Technology, Kluver Academic Publisher, Netherlands, 1996.

[47] X. Zhang, J. Hu, Q. Chang, Y. Wang, J.e. Zhou, T. Zhao, Y. Jiang, X. Liu, Influences of internal coagulant composition on microstructure and properties of porous YSZ hollow fibre membranes for water treatment, Sep. Purif. Technol. 147 (2015) 337-345.

[48] M. Lee, Z. Wu, B. Wang, K. Li, Micro-structured alumina multi-channel capillary tubes and monoliths, J. Membr. Sci. 489 (2015) 64-72.

[49] C.C. Wei, O.Y. Chen, Y. Liu, K. Li, Ceramic asymmetric hollow fibre membranes—One step fabrication process, J. Membr. Sci. 320 (2008) 191-197.

[50] E. Gbenedio, Z. Wu, I. Hatim, B.F.K. Kingsbury, K. Li, A multifunctional Pd/alumina hollow fibre membrane reactor for propane dehydrogenation, Catal. Today 156 (2010) 93-99.

[51] X. Tan, N. Liu, B. Meng, S. Liu, Morphology control of the perovskite hollow fibre membranes for oxygen separation using different bore fluids, J. Membr. Sci. 378 (2011) 308-318.

[52] K.R. Reddy, V.G. Gomes, M. Hassan, Carbon functionalized TiO2 nanofibers for high efficiency photocatalysis, Mater. Res. Express 1 (2014) 015012.

[53] J. Kujawa, S. Cerneaux, W. Kujawski, Highly hydrophobic ceramic membranes applied to the removal of volatile organic compounds in pervaporation, Chem. Eng. J. 260 (2015) 43-54.

[54] J. Kujawa, W. Kujawski, S. Koter, K. Jarzynka, A. Rozicka, K. Bajda, S. Cerneaux, M. Persin, A. Larbot, Membrane distillation properties of TiO2ceramic membranes modified by perfluoroalkylsilanes, Desalin. Water Treat. 51 (2013) 1352-1361.

[55] J. Kujawa, S. Cerneaux, W. Kujawski, Characterization of the surface modification process of Al2O3, TiO2 and ZrO2 powders by PFAS molecules, Colloids Surf., A 447 (2014) 14-22.

[56] J.A. Sanmartino, M. Khayet, M.C. García-Payo, H. El Bakouri, A. Riaza, Desalination and concentration of saline aqueous solutions up to supersaturation by air gap membrane distillation and crystallization fouling, Desalination 393 (2016) 39-51.

[57] A. Larbot, L. Gazagnes, S. Krajewski, M. Bukowska, K. Wojciech, Water desalination using ceramic membrane distillation, Desalination 168 (2004) 367-372.

[58] C. Ren, H. Fang, J. Gu, L. Winnubst, C. Chen, Preparation and characterization of hydrophobic alumina planar membranes for water desalination, J. Eur. Ceram. Soc. 35 (2015) 723-730.

[59] J.W. Zhang, H. Fang, L.Y. Hao, X. Xu, C.S. Chen, Preparation of silicon nitride hollow fibre membrane for desalination, Mater. Lett. 68 (2012) 457-459.

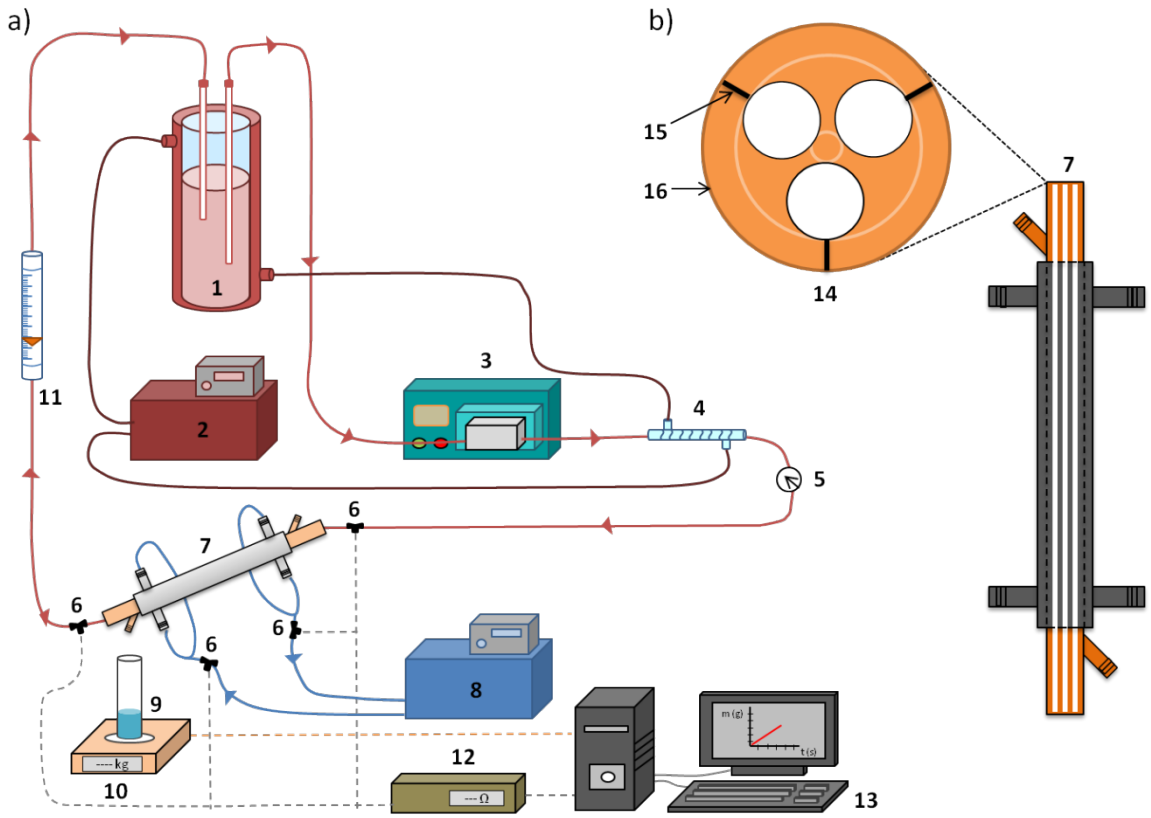

Fig. 1. a) AGMD experimental set-up: (1) Feed; (2) heating thermostat; (3) peristaltic pump; (4) glass heat exchanger; (5) pressure gauge; (6) Pt-100 probes; (7) hollow fiber membrane module; (8) cooling thermostat; (9) permeate; (10) balance; (11) flow meter; (12) multimeter; (13) computer; b) hollow fiber membrane module: (14) three-holed cover; (15) minimum air gap width = 1 mm; (16) condensation surface.

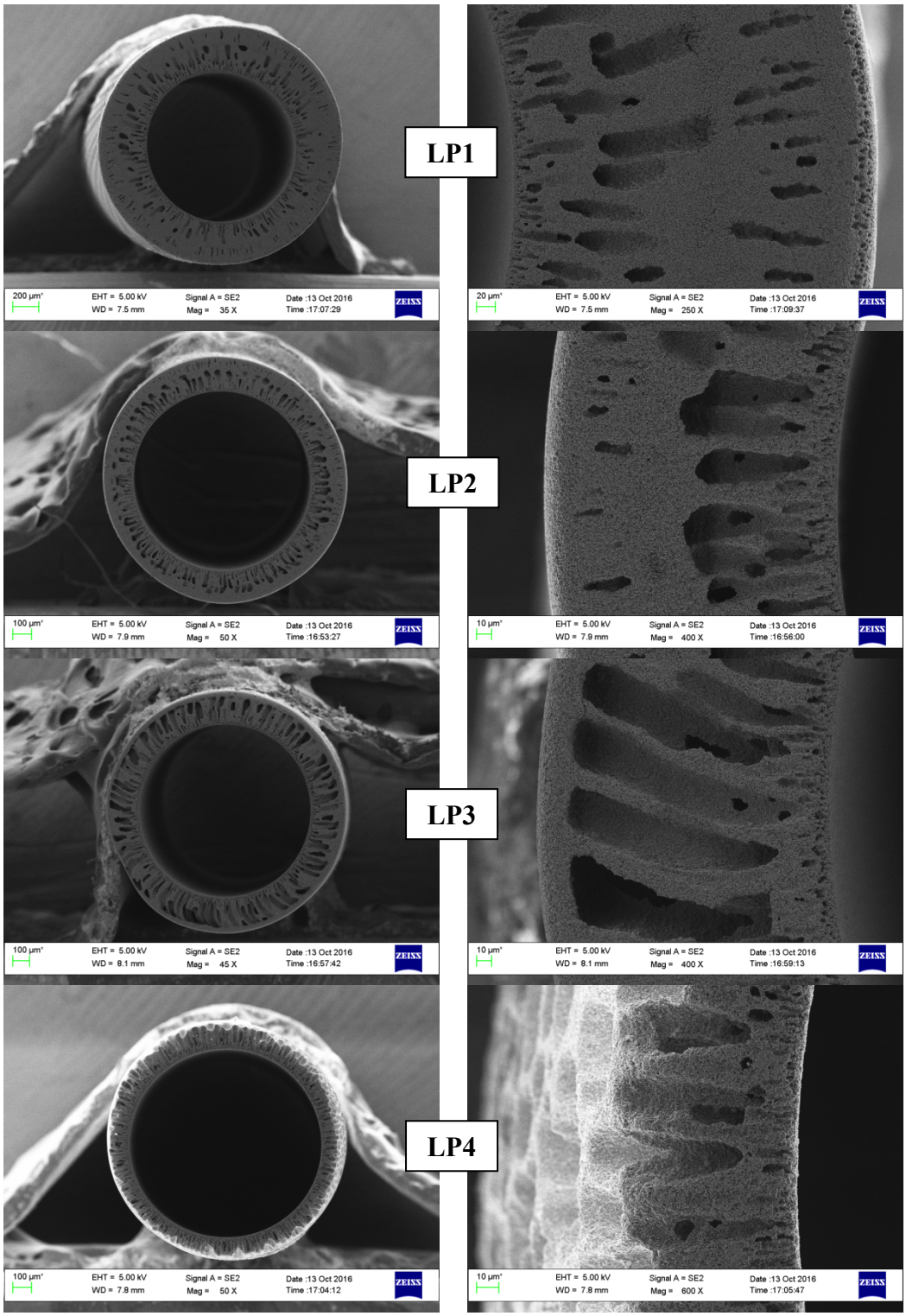

Fig. 2. SEM cross-section images of the alumina hollow fiber membranes prepared with the LP inorganic suspension.

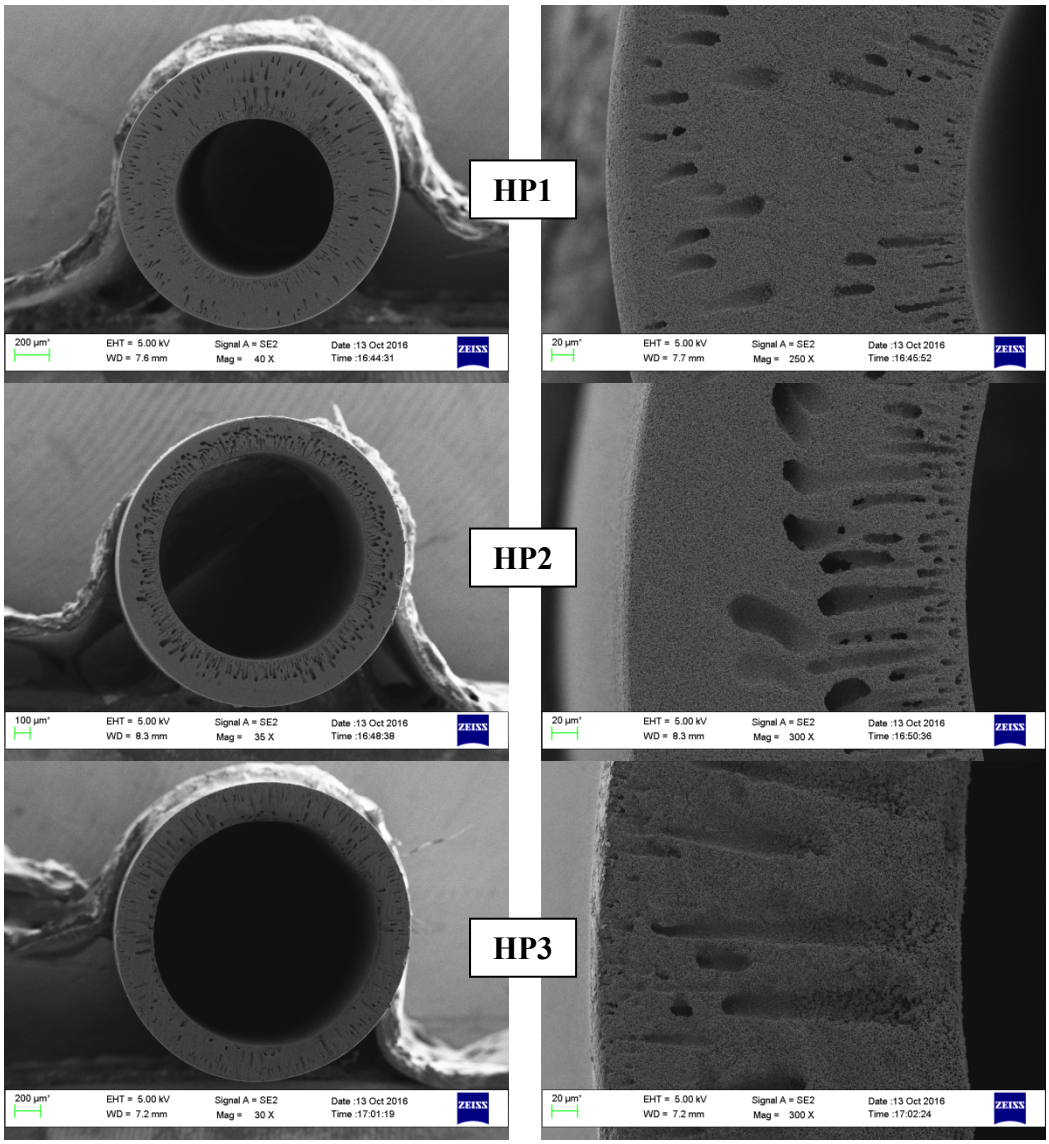

Fig. 3. SEM cross-section images of the alumina hollow fiber membranes prepared with HP inorganic suspension.

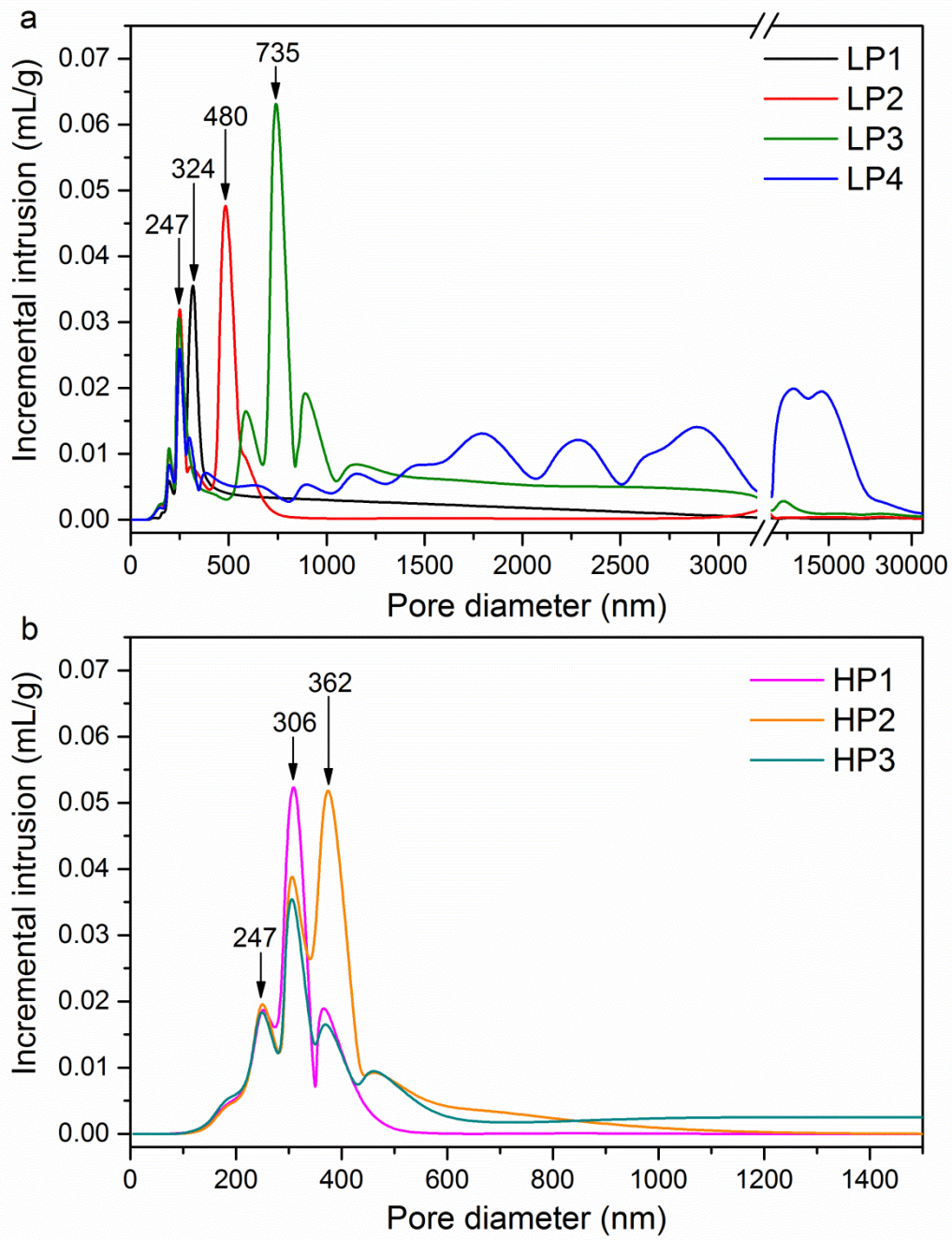

Fig. 4. Pore size distributions of the original alumina hollow fiber membranes prepared with the LP suspension (a) and the HP suspension (b) determined by MIP analysis.

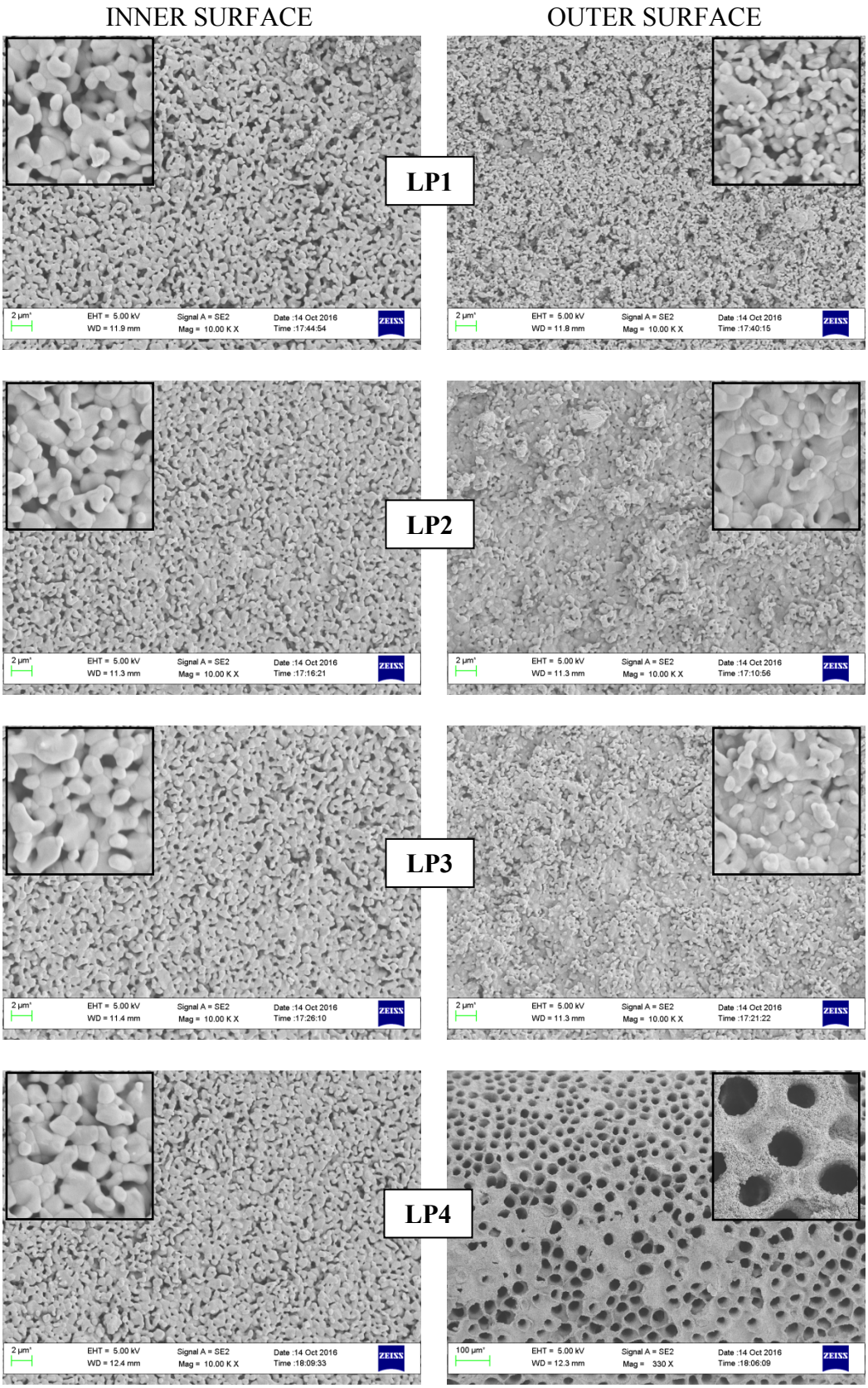

Fig. 5. SEM surface images of the alumina hollow fiber membranes prepared with the LP inorganic suspension.

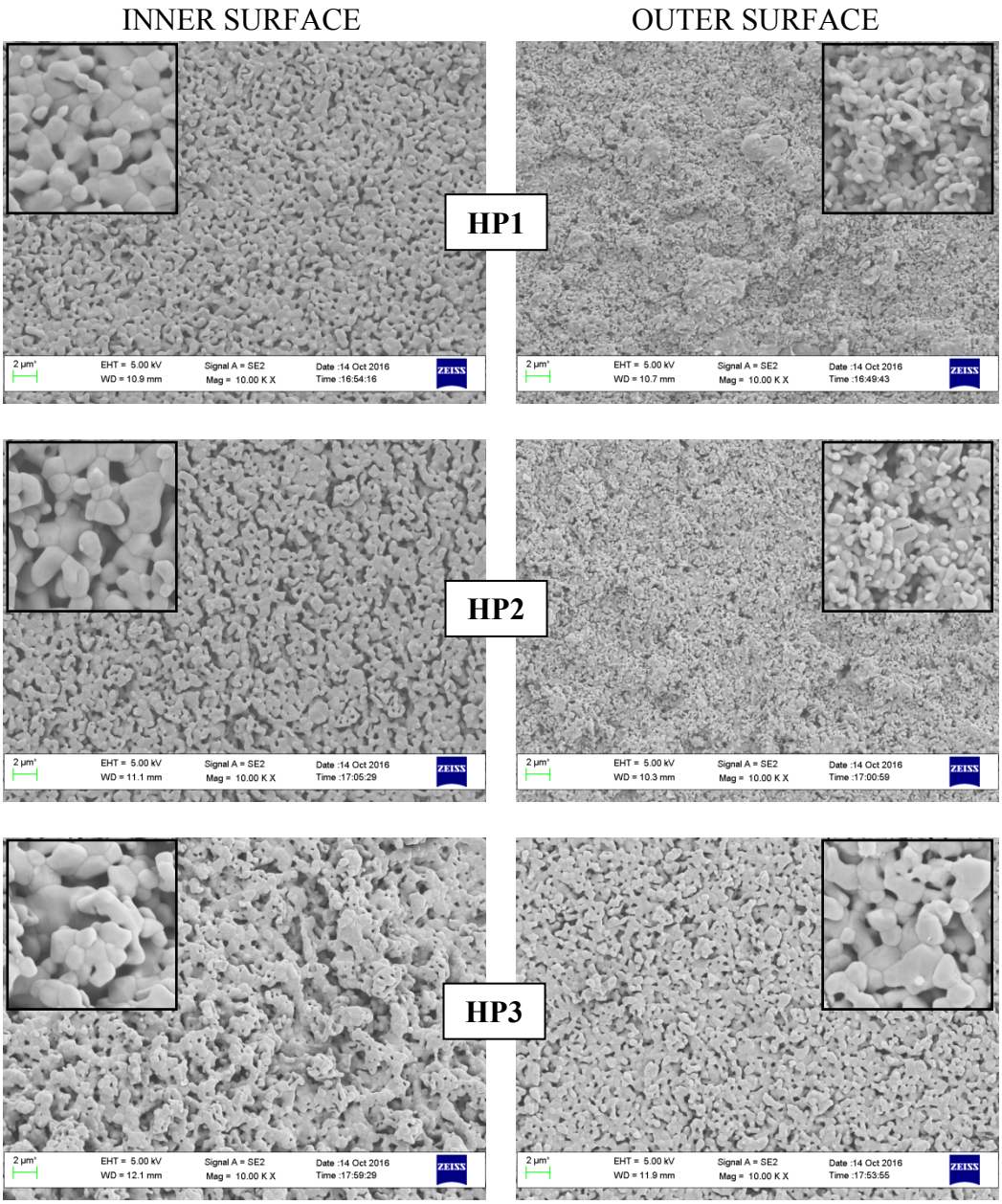

Fig. 6. SEM surface images of the alumina hollow fiber membranes prepared with the HP inorganic suspension.

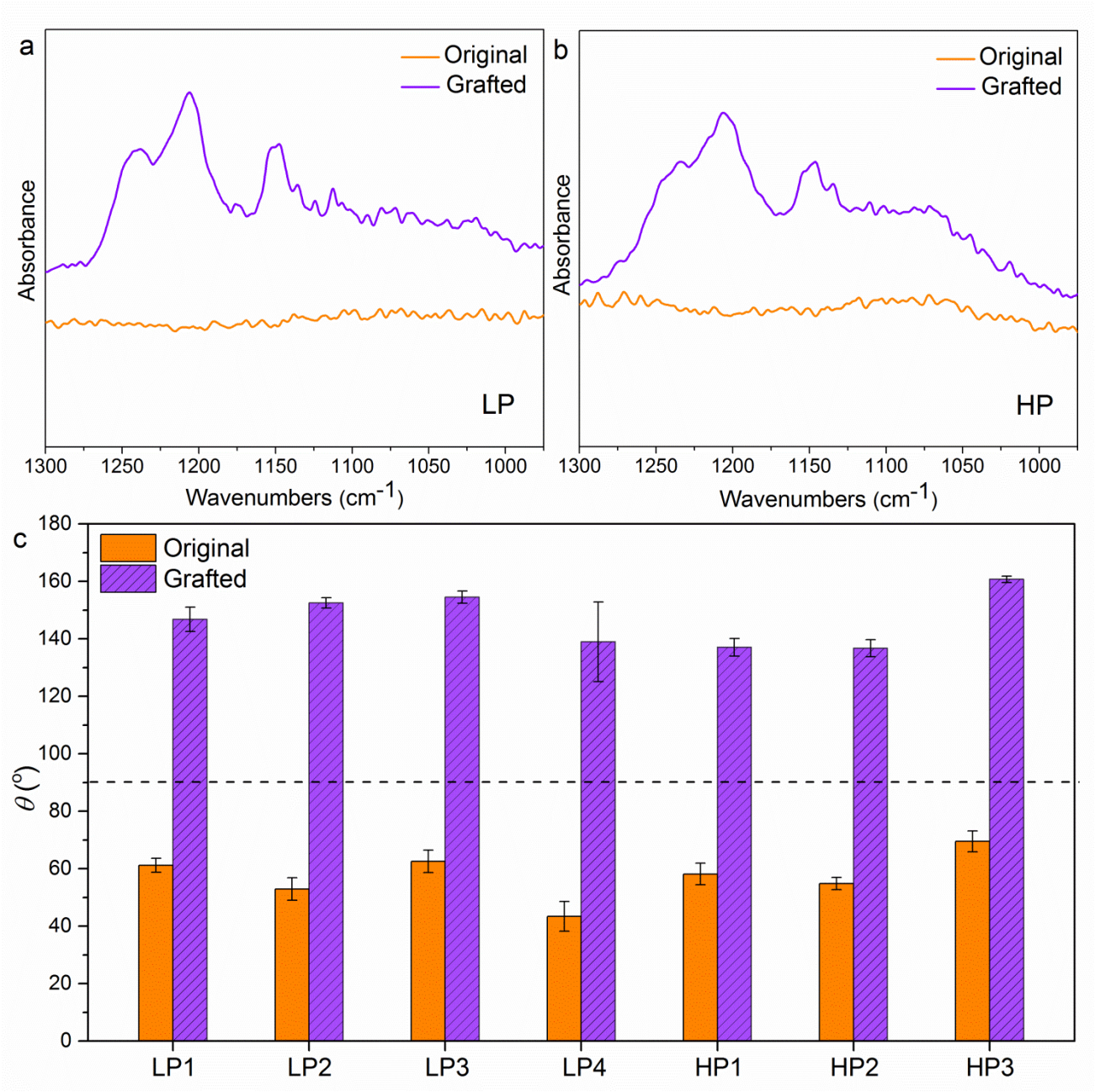

Fig. 7. FTIR-ATR spectra (a, b) and advancing contact angles (c) of the prepared alumina hollow fiber membranes before and after grafting modification. FTIR-ATR spectra of the membranes prepared with LP suspension (a) and the HP suspension (b).

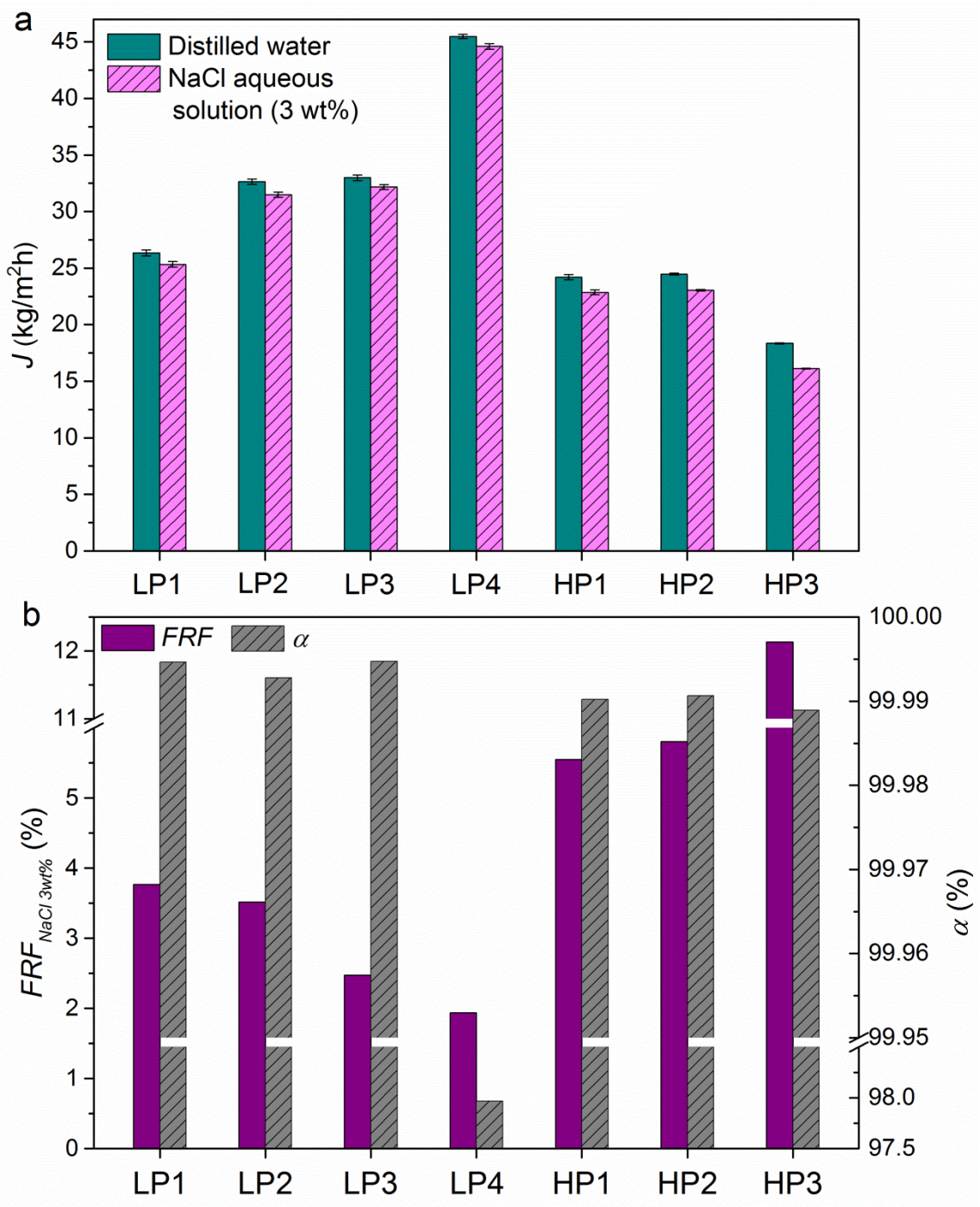

Fig. 8. AGMD (a) permeate flux (J) and (b) permeate flux reduction factor (FRF) and salt rejection factor (α) at 3 wt% NaCl feed aqueous solution, of the grafted alumina hollow fiber membranes.

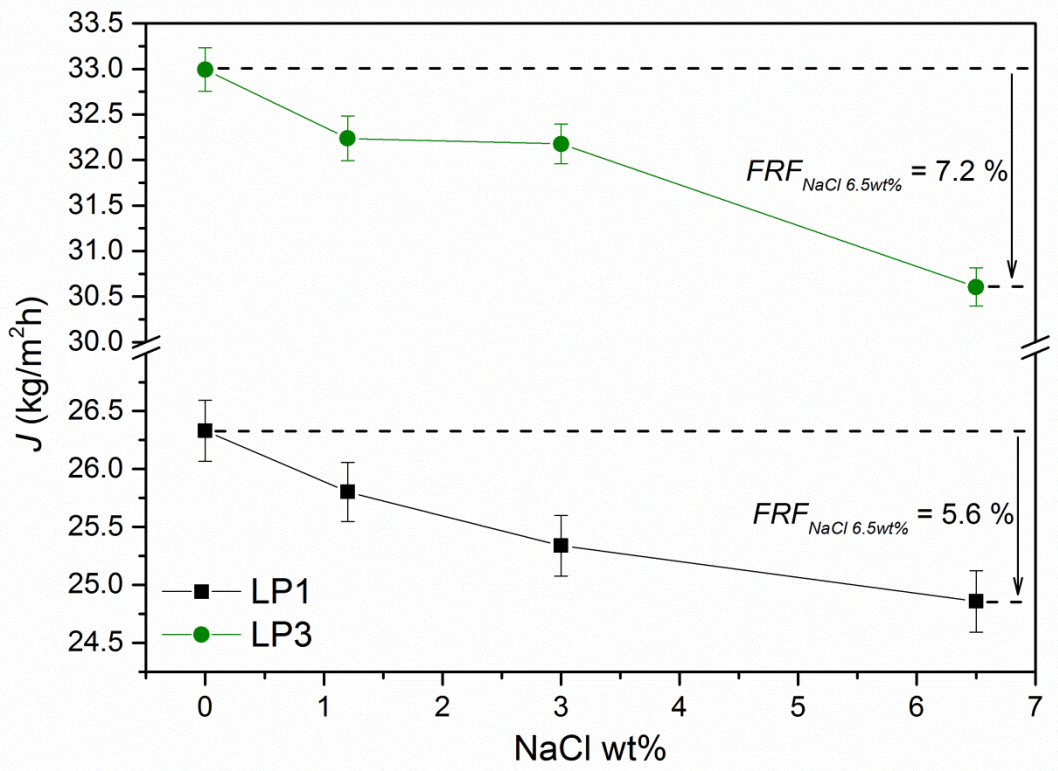

Fig. 9. Effect of the NaCl concentration of the feed solution on the AGMD permeate flux (*J*) of the grafted alumina hollow fiber membranes LP1 and LP3.

Table 1. Spinning parameters of alumina hollow fiber membranes.

Inorganic suspension (IS)	Membrane	IS flow rate (ml/min)	Bore liquid (BL)	BL flow rate (ml/min)	Outer coagulant (OC)	OC flow rate (ml/min)	Gap distance (cm)
LP	LP1	15	DI water	10	N.A.	N.A.	0
	LP2	8	DI water	10	Ethanol/NMP (50/50 wt%)	4	5
	LP3	8	DI water	15	Ethanol/NMP (50/50 wt%)	4	5
	LP4	8	DI water	30	NMP	5	25
HP	HP1	8	DI water	10	Ethanol/NMP (50/50 wt%)	4	5
	HP2	8	DI water	15	Ethanol/NMP (50/50 wt%)	4	5
	HP3	8	Ethanol/NMP (40/60 wt%)	12	N.A.	N.A.	0

Table 2. Diameters and thickness of the alumina hollow fiber membranes.

Membrane	Inner diameter (μm)	Outer diameter (μm)	Thickness (μm)
LP1	1102 ± 11	1809 ± 17	354 ± 7
LP2	921 ± 6	1282 ± 18	180 ± 4
LP3	974 ± 6	1337 ± 13	181 ± 3
LP4	1003 ± 3	1293 ± 9	145 ± 1
HP1	1075 ± 10	1701 ± 10	313 ± 5
HP2	1417 ± 4	1953 ± 10	268 ± 2
HP3	1812 ± 3	2308 ± 12	248 ± 2

Table 3. Bubble pore size, mean pore size, and smallest pore size of the alumina hollow fiber membranes before and after grafting determined by gas-liquid displacement test.

Membrane	Bubble pore size (nm)		Mean pore size (nm)		Smallest pore size (nm)	
	Original	Grafted	Original	Grafted	Original	Grafted
LP1	340 ± 14	344 ± 15	237 ± 6	250 ± 16	203.7 ± 0.7	220 ± 18
LP2	270.0 ± 0.6	288.7 ± 1.2	231.4 ± 0.8	232 ± 3	213 ± 17	195 ± 15
LP3	267.2 ± 1.2	280 ± 14	228.0 ± 0.7	227 ± 3	222.1 ± 0.5	185 ± 30
LP4	1085 ± 50	1181 ± 40	537 ± 29	556 ± 22	490 ± 50	434 ± 33
HP1	345.15 ± 0.21	370 ± 3	229 ± 8	223 ± 3	189 ± 15	193 ± 18
HP2	332.6 ± 0.9	360.4 ± 1.2	247.6 ± 1.7	255 ± 7	198 ± 15	205 ± 10
HP3	382.1 ± 27	369.8 ± 1.8	228 ± 16	251 ± 11	177 ± 3	175 ± 7

Table 4. Tortuosity factor of the original alumina hollow fiber membranes determined by MIP technique and void volume fraction (i.e. porosity) (ε) of the original and grafted fibers determined by gravimetric method.

Membrane	Tortuosity factor	ε (%)	
		Original	Grafted
LP1	1.801	50.5 ± 0.7	48.6 ± 0.5
LP2	1.814	54.4 ± 1.3	57.0 ± 1.1
LP3	1.706	55.5 ± 1.1	57.0 ± 1.9
LP4	1.782	70.4 ± 0.4	74.8 ± 2.2
HP1	1.794	48.1 ± 1.3	50.3 ± 2.7
HP2	1.738	51.7 ± 1.2	54.6 ± 1.2
HP3	1.817	51.0 ± 1.3	50.3 ± 1.4

Table 5. Bending strength (σ_F) of the original alumina hollow fiber membranes.

Membrane	σ_F (MPa)
LP1	142 ± 7
LP2	150 ± 14
LP3	110 ± 8
LP4	50 ± 5
HP1	156 ± 12
HP2	120 ± 8
HP3	183 ± 10

Table 6. Reported MD performance of different types of grafted ceramic membranes.

MD configuration	Membrane material (grafting agent)	Membrane shape	Feed solution and temperatures (feed, T_f; permeate, T_p; cooling, T_c)	Permeate flux (L m^{-2} h^{-1})	Separation factor (%)	Ref
AGMD	Alumina, Al200 (1H, 1H, 2H, 2H-perfluorodecyltriethoxysilane, T-PFS)	Tubular	3 - 6 wt% NaCl T_f = 95 °C T_c = 25 °C	5.03 (3 wt%) 4.16 (6 wt%)	99.6 (3 wt%) 90.7 (6 wt%)	[18]
	Zirconia, Zr50 (T-PFS)			5.25 (3 wt%) 4.59 (6 wt%)	100	
AGMD	Clay-alumina, C-55-M (T-PFS)	Capillary	3 wt% NaCl T_f = 70 °C T_c = 10 °C	4.1	99.96	[16]
AGMD	Zirconia layer/alumina support, M3 (T-PFS)	Tubular	Pure water (0 wt%) - 6 wt% NaCl T_f = 99 °C T_p = 5 °C	6.25 (0 wt%) 5.42 (6 wt%)	100	[13]
AGMD	Titania, Ti-300kD-tC6 (1H,1H,2H,2H-perfluorooctyltriethoxysilane, T-PFOS)	Tubular	3 wt% NaCl T_f = 90 °C T_p = 5 °C	3.7	N.A.	[14]
AGMD	Alumina, LP3 (T-PFS)	Hollow fiber	0 - 1.2 - 3 - 6.5 wt% NaCl T_f = 80 °C T_c = 20 °C	33.0 (0 wt%) 32.2 (1.2 wt%) 32.1 (3 wt%) 30.6 (6.5 wt%)	>99.99	This study
AGMD	Zirconia, Zr50 (T-PFS)	Tubular	3 wt% NaCl T_f = 95 °C T_c = 5 °C	4.7	99.8	[19]

DCMD			3 wt% NaCl T_f = 95 °C T_c = 5 °C	4	99.8	
VMD			3 wt% NaCl T_f = 40 °C Pressure = 3 mbar	7.5	96.1	
DCMD	Alumina (T-PFS)	Tubular	0.6 - 6 wt% NaCl T_f = 95 °C T_p = 5 °C	6.8 (0.6 wt%) 5.4 (6 wt%)	100	[57]
DCMD	Alumina (T-PFOS)	Planar	2 - 4 - 6 wt% NaCl T_f = 80 °C T_p =20 °C	19.1 (2 wt%) 17.0 (4 wt%) 15.5 (6 wt%)	> 99.5 (2 wt%)	[58]
DCMD	Alumina, Anodisc-200 (T-PFS)	Planar	0.6 wt% NaCl T_f= 53 °C T_p = 18 °C	17 - 8	93 - 99	[15]
DCMD	Silicon Nitride (T-PFOS)	Hollow fiber	0.5 - 2 - 4 - 6 wt% NaCl T_f = 80 °C T_p = 20 °C)	13.4 (0.5 wt%) 12.2 (2 wt%) 11.0 (4 wt%) 9.0 (6 wt%)	99 - 100	[8]
VMD			0.5 – 2 – 4 - 6 wt% NaCl T_f = 80 °C Pressure = 0.02 bar	36.7 (0.5 wt%) 32.1 (2 wt%) 28.3 (4 wt%) 23.7 (6 wt%)		
DCMD	β-Sialon, $Si_{6-z}Al_zO_zN_{8-z}$, z = 2 (T-PFOS)	Hollow fiber	2 - 4 wt% NaCl T_f = 80 °C T_p = 20 °C	7.9 (2 wt%) 6.8 (4 wt%)	99 - 100	[17]

VMD			2 - 4 wt% NaCl T_f = 80 °C Pressure = 0.02 bar	12.2 (2 wt%) 10.75 (4 wt%)		
VMD	Alumina (T-PFOS)	Hollow fiber	2 - 4 - 6 wt% NaCl T_f = 80 °C Pressure = 0.04 bar	45 (2 wt%) 42.9 (4 wt%) 41 (6 wt%)	> 99.5 (4 wt%)	[6]
VMD	Silicon Nitride (T-PFOS)	Hollow fiber	2 - 4 wt% NaCl T_f = 70 °C Pressure = 0.02 bar	25 (2 wt%) 22.25 (4 wt%)	99 - 100	[59]